ARL-TR-7768 ● SEP 2016


US Army Research Laboratory

# The First Static and Dynamic Analysis of 3-D Printed Sintered Ceramics for Body Armor Applications

by Tyrone L Jones, Jeffrey Swab, Christopher S Meredith, and Benjamin Becker

## NOTICES

### Disclaimers

The findings in this report are not to be construed as an official Department of the Army position unless so designated by other authorized documents.

Citation of manufacturer's or trade names does not constitute an official endorsement or approval of the use thereof.

Destroy this report when it is no longer needed. Do not return it to the originator.

ARL-TR-7768 ● SEP 2016

US Army Research Laboratory

# The First Static and Dynamic Analysis of 3-D Printed Sintered Ceramics for Body Armor Applications

**by Tyrone L Jones, Jeffrey Swab, and Christopher S Meredith**
*Weapons and Materials Research Directorate, ARL*

**Benjamin Becker**
*HotEnd Works, LLC, Oberlin, Ohio*

# REPORT DOCUMENTATION PAGE

*Form Approved*
*OMB No. 0704-0188*



| 1. REPORT DATE *(DD-MM-YYYY)* | 2. REPORT TYPE | 3. DATES COVERED (From - To) |
|---|---|---|
| September 2016 | Technical Report | August 2014–December 2015 |

**4. TITLE AND SUBTITLE**
The First Static and Dynamic Analysis of 3-D Printed Sintered Ceramics for Body Armor Applications

**5a. CONTRACT NUMBER**

**5b. GRANT NUMBER**

**5c. PROGRAM ELEMENT NUMBER**

**6. AUTHOR(S)**
Tyrone L Jones, Jeffrey Swab, Christopher S Meredith, and Benjamin Becker

**5d. PROJECT NUMBER**

**5e. TASK NUMBER**

**5f. WORK UNIT NUMBER**

**7. PERFORMING ORGANIZATION NAME(S) AND ADDRESS(ES)**
US Army Research Laboratory
ATTN: RDRL-WMP-E
Aberdeen Proving Ground, MD 21005-5069

**8. PERFORMING ORGANIZATION REPORT NUMBER**
ARL-TR-7768

**9. SPONSORING/MONITORING AGENCY NAME(S) AND ADDRESS(ES)**

**10. SPONSOR/MONITOR'S ACRONYM(S)**

**11. SPONSOR/MONITOR'S REPORT NUMBER(S)**

**12. DISTRIBUTION/AVAILABILITY STATEMENT**
Approved for public release; distribution is unlimited.

**13. SUPPLEMENTARY NOTES**

**14. ABSTRACT**
Traditional manufacturing of ceramics used for ballistic impact protection presents limitations of long lead times, fabrication of complex geometries, and expensive components. Ceramic 3-D printing offers engineering-grade ceramic components in approximately 90% less time than traditional ceramics. Typical turnaround can be in days, instead of weeks, depending on the complexity of the part. This not only allows for faster time to market, but also allows for more iterations during the design process, resulting in a better end product. Additionally, 3-D printed parts can have a higher degree of complexity for weight reduction while saving on the cost of the part because of the reduction in material used.

The US Army Research Laboratory collaborated with HotEnd Works, LLC, of Oberlin, Ohio, to evaluate sintered alumina tiles produced by 3-D printing methodology. This report examines the static and quasi-static parameters (including density, hardness, and fracture strength) and semi-infinite penetration performance of 3-D printed sintered alumina. These results are compared with traditionally sintered alumina.

**15. SUBJECT TERMS**
body armor, 3-D printed ceramics, alumina, additive manufacturing, ballistic impact, low-speed impact

| 16. SECURITY CLASSIFICATION OF: | | | 17. LIMITATION OF ABSTRACT | 18. NUMBER OF PAGES | 19a. NAME OF RESPONSIBLE PERSON |
|---|---|---|---|---|---|
| a. REPORT | b. ABSTRACT | c. THIS PAGE | | | Tyrone L Jones |
| Unclassified | Unclassified | Unclassified | UU | 36 | 19b. TELEPHONE NUMBER (Include area code) (410) 278-6223 |

## Contents


List of Figures iv

List of Tables iv

Acknowledgments v

1. Introduction 1

2. Processing and Experimental Procedures 1

3. Results and Discussion 7

4. Conclusions 19

5. References 21

Appendix. Videos 23

List of Symbols, Abbreviations, and Acronyms 25

Distribution List 26

## List of Figures


Fig. 1 Typical die press assembly ....2
Fig. 2 PSD technology ....3
Fig. 3 Alumina tiles before impact....4
Fig. 4 Sketch of ceramic composite samples ....4
Fig. 5 Initial conditions of ceramic composite samples in fixture ....5
Fig. 6 Cross section of a 12.7-mm APM2....5
Fig. 7 Measurement of residual penetration....6
Fig. 8 Experimental setup for recording fracture ....7
Fig. 9 Rod projectile....7
Fig. 10 Representative microstructure of A) AD-995 and B) HEW alumina ....8
Fig. 11 Ballistic penetration into AA6061 ....9
Fig. 12 Penetration of 12.7-mm APM2 into AA6061....10
Fig. 13 Residual penetrator from impact versus CoorsTek alumina AD-995..11
Fig. 14 Residual penetrator from impact versus HEW alumina ....12
Fig. 15 Residual mass of 12.7-mm APM2 into AA6061 ....12
Fig. 16 Residual length of 12.7-mm APM2 into AA6061 ....13
Fig. 17 CoorsTek alumina AD-995 after impact....13
Fig. 18 HEW alumina after impact ....14
Fig. 19 Ceramic performance map....15
Fig. 20 Progressive fracture of the 6-mm ceramic: a) CoorsTek and b) HEW ....16
Fig. 21 Progressive fracture of the 8-mm ceramic: a) CoorsTek and b) HEW ....18


## List of Tables


Table 1 Property summary....8
Table 2 Ballistic impact measurements for alumina tiles ....11
Table 3 Comparative performance of ceramics ....14
Table 4 Comparison of the dynamic failure modes of 6-mm-thick alumina discs....17
Table 5 Comparison of the dynamic failure modes of 8-mm-thick alumina discs....19

## Acknowledgments

Thanks to Ron Worthington for setting up and contributing to the low-speed impact experiments.

INTENTIONALLY LEFT BLANK.

## 1. Introduction

Traditional manufacturing of ceramics used for ballistic impact protection presents limitations of long lead times, fabrication of complex geometries, and expensive components. Ceramic 3-D printing offers engineering-grade ceramic components in approximately 90% less time than traditional ceramics manufacturing. Typical turnaround can be in days, instead of weeks, depending on the complexity of the part. This not only allows for faster time to market, but also allows for more iterations during the design process, resulting in a better end product. Additionally, 3-D printed parts can have a higher degree of complexity for weight reduction while saving on the cost of the part because less material is required.

The US Army Research Laboratory collaborated with HotEnd Works, LLC (HEW), of Oberlin, Ohio, to evaluate sintered alumina tiles produced by 3-D printing methodology. This report examines the static and quasi-static parameters (including density, hardness, and fracture strength), semi-infinite penetration performance, and the fracture profile following impact of 3-D printed sintered alumina. These results are compared with traditionally sintered alumina, which are used as the ceramic baseline performance.

While typical US body armor tends to use higher-performance ceramics (such as boron carbide), this program examined 8-mm-thick alumina as the initial, cost-effective material for evaluation of the depth of penetration (DOP). Additionally, 6- and 8-mm-thick alumina were used to develop a deeper understanding of the stages of ceramic failure caused by a small steel rod at a low-speed impact. Rod-shaped specimens, nominally 3 mm in diameter and 50 mm long, were obtained for each alumina to quantify static and quasi-static material properties. The following ceramics were evaluated:

- Traditionally manufactured, sintered alumina AD-995 (also sometimes called CAP3) from CoorsTek, Golden, Colorado.
- 3-D printed sintered alumina from HEW.

## 2. Processing and Experimental Procedures

Traditional manufacturing of advanced ceramics typically employs various methods, the most common being die pressing or isopressing of a ceramic powder that has been combined with binding and plasticizing components.[1] To form the powder into the desired shape, tooling must be created that replicates the geometry of the components (Fig. 1). If the geometry of the component is beyond a basic

shape such as a rectangle, square, or cylinder, secondary green machining using a Computer Numerical Control mill or lathe is required. Traditional manufacturing of a simple rectangle involves die pressing or isopressing of a prepared ceramic powder using rectangular tooling (die). The die is unloaded, and the part is then sintered at its respective densification temperature (i.e., for alumina this would be approximately 1,600 °C). If there are stringent requirements in terms of flatness, parallelism, or perpendicularity of surfaces, the component needs to be ground using diamond tooling after the sintering process.[1]

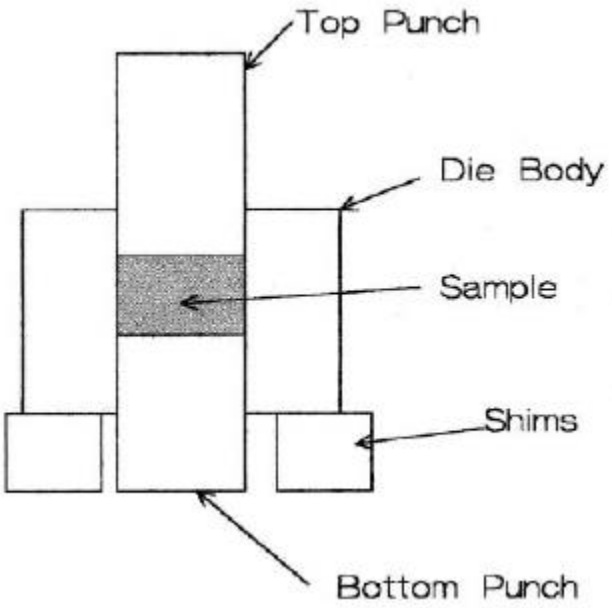


**Fig. 1 Typical die press assembly**

Additive manufacturing of advanced ceramics differs mostly in terms of the initial green part formation when compared with a traditional manufacturing process. The process used by HEW is pressurized spray deposition (PSD). The PSD process (Fig. 2) involves the use of a proprietary blend of advanced ceramic raw material (ceramic powder) with a unique polymeric binder (support material). The polymeric support material serves as a temporary support structure during part formation to accommodate overhangs and other intricate features.[2] Powder and support materials are fed from external hoppers into the dispensing chambers and then deposited by a high-precision deposition nozzle. The deposition nozzle uses mechanical shaping methods that allow for a range of patterns from 0.127 to 3.81 mm (0.005 to 0.150 inch) in diameter. After the first layer is complete, formation of the next layer initiates.

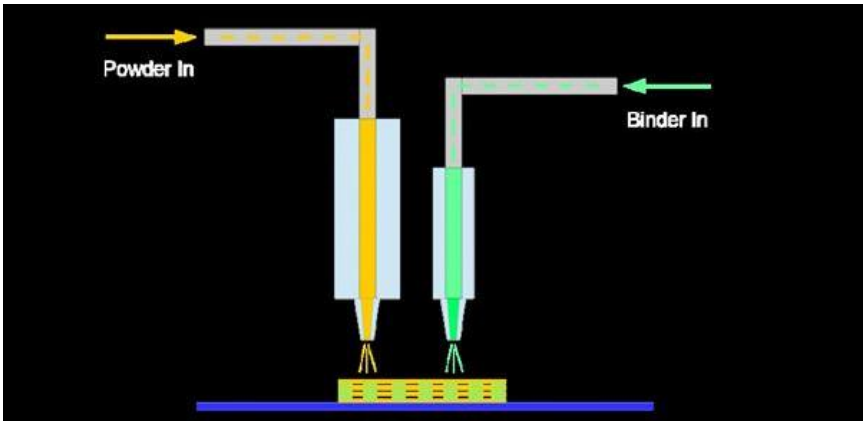


**Fig. 2 PSD technology**

After the formation of the component, a thermal debinding process takes place. Thermal debinding of the component is done within a wicking embedment, with an average cycle time of 24 h. The thermal debinding temperature does not exceed 150 °C. Due to the type of embedment material used, the part does not require cleaning when it is removed from the thermal debinding oven. After debinding, the component is then processed using a traditional electric or gas furnace to complete the densification. Because shrinkage occurs with the additive ceramic process, postprocessing such as diamond grinding may be required for components with tight tolerance requirements in terms of flatness and the like. However, tooling fabrication as well as the green machining stage can be omitted due to the geometric complexity that is possible with the PSD process.

DOP or residual penetration experiments were designed to determine the relative ballistic performance of different ceramic materials shown in Fig. 3.[3] For DOP testing, a projectile is fired into a ceramic tile attached to a semi-infinite thick metal plate such that the projectile penetrates through the ceramic tile and then into the metal plate without deforming the back surface. These experiments avoid the fundamental problem of $V_{50}$ ballistic dependence on armor design (e.g., front-to-back plate ratio and material), require fewer shots than $V_{50}$ tests, and have a sensitivity equivalent to that of other ballistic test methods.[4] The change in penetration into the metal plates provides a comparison by which to rank the performance of the ceramic materials. The target configuration used for these experiments is illustrated in Figs. 4 and 5. The target consisted of a 90- × 90-mm ceramic tile at a nominal thickness of 8 mm, backed by 2 aluminum alloy 6061 (AA6061, MIL-DTL-32262) plates of 50.8-mm (2-inch) thickness.[5] An epoxy resin, Dureflex Optical Aliphatic Polyether Polyurethane Grade A4700, was used to attach each tile to the front surface of the first 50.8-mm (2-inch) plate. AA6061

was chosen as a well-characterized and readily available residual penetration material. The aluminum plates were also expected to provide better resolution than steel backer plates. No cover plate was employed.

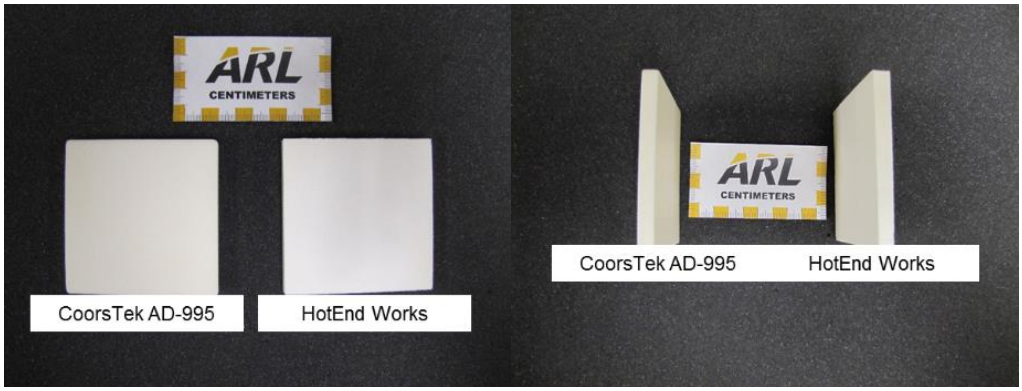


**Fig. 3 Alumina tiles before impact**

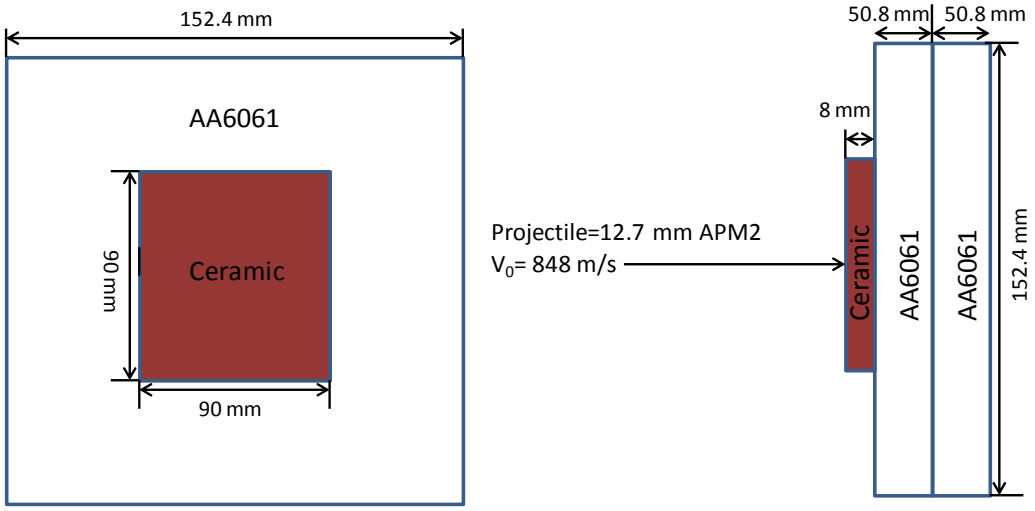


**Fig. 4 Sketch of ceramic composite samples**

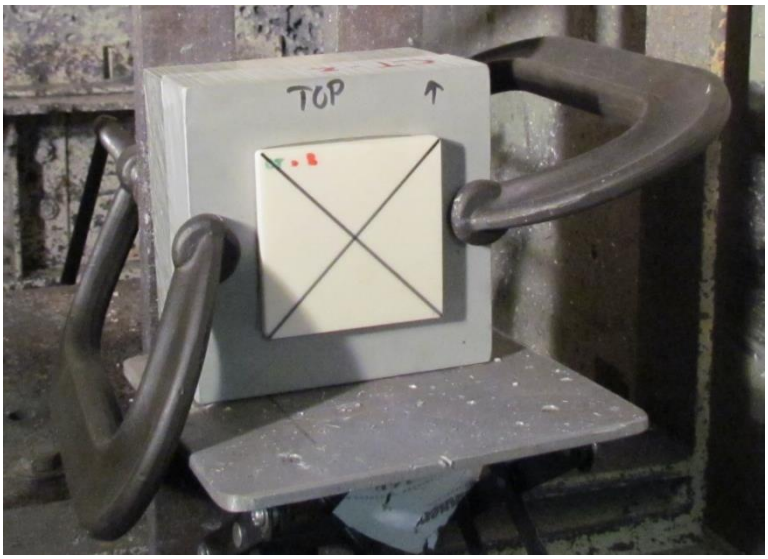


**Fig. 5 Initial conditions of ceramic composite samples in fixture**

All ballistic impact experiments were conducted at the US Army Research Laboratory. Three experiments were performed for each alumina manufacturing process. The test projectile was the copper-jacketed 12.7-mm APM2, which includes a hardened steel core penetrator with a length of 47.6 mm (1.875 inches), a diameter of 10.87 mm (0.428 inch), and an aspect ratio of 4 (Fig. 6). The nominal projectile weight was 46 g, and core density was 7.85 g/cm$^3$.

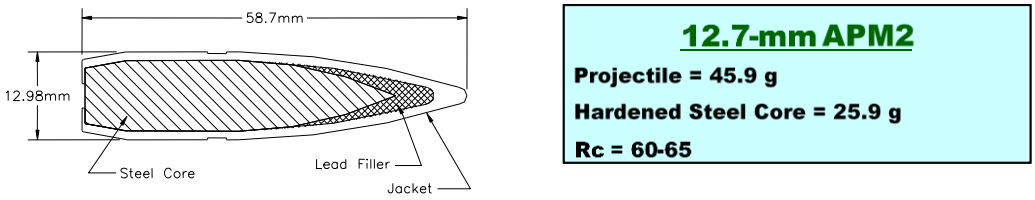


**Fig. 6 Cross section of a 12.7-mm APM2**

The impact velocity used for all experiments was nominally 848 m/s (2,782 ft/s), although some shots varied from 824 m/s (2,704 ft/s) up to 872 m/s (2,861 ft/s). This variability could be due to interior barrel conditions, differences in the APM2 material properties, or gun operator influence such as projectile powder measurements. The impact velocity was intentionally chosen to produce a range of measureable residual penetrations while being consistent with real-world ballistic impact conditions. Measurement of the projectile yaw and velocity was accomplished using a Hewlett-Packard 150-kV Flash X-ray Imaging System in 2 orthogonal planes. All residual penetration measurements were obtained by sectioning the AA6061 plates to reveal a cross section. Electrical discharge machining (EDM) was used to section all penetration cavities, and measurements

were made using vernier calipers to the deepest portion at the cavity, as indicated in Fig. 7.[3] Measurement of the "a" value avoids errors that could be caused by deformation of the aluminum block around the cavity entrance.[6]

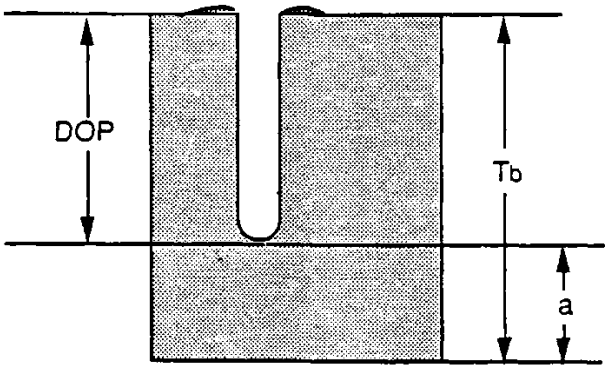


**Fig. 7 Measurement of residual penetration**

Additional experiments were performed to qualitatively assess the fracture propagation of the alumina with a high-speed camera due to low-speed impact by a small rod-shaped projectile. Tiles of 2 thicknesses, 6 and 8 mm, were impacted at approximately 210 m/s due to limitations with the gas gun used. Thus, direct comparisons with the ballistic tests may be dubious. The experimental setup is shown in Fig. 8. The approximately 44-mm-diameter alumina samples were held in a 3-screw adjustable ring mount. A section of the ring was cut out so that the high-speed camera could view the side of the sample. A mirror was placed behind the sample and was angled such that the back-face of the sample was visible in the frame (not shown in the figure). The alumina sample was aligned such that the face was perpendicular to axis of the gun barrel. The high-speed camera was a Shimadzu HPV-X2 recording at 1 million frames per second with an exposure time of 200 ns. The projectile was a 3.18-mm-diameter × 35-mm-long, right-circular cylinder rod. Figure 9 shows a photo of the projectile with the sabot. The projectile weighed 7.5 g, including the weight of the foam sabot. Each line in the photo is 10 mm. The projectile is made of hardened M2 steel with a Rockwell C hardness of 62. The hardness is similar to the hardness of the APM2 projectile. A machinable foam sabot was used to hold the rod as it accelerated down the larger diameter gun barrel. Velocity was measured using a pair of lasers and detectors at the end of the barrel; the constant voltage signal from the detectors dropped to zero when the projectile blocked the laser beam. One of the laser beams was also used as a trigger, initiating the recording by the camera.

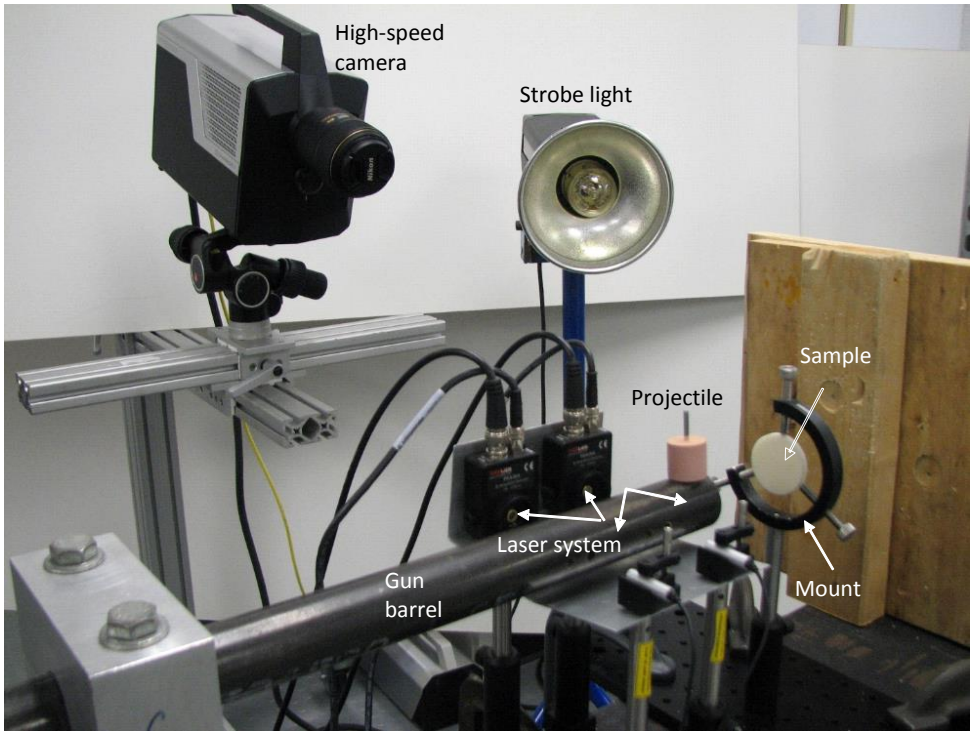


**Fig. 8 Experimental setup for recording fracture**

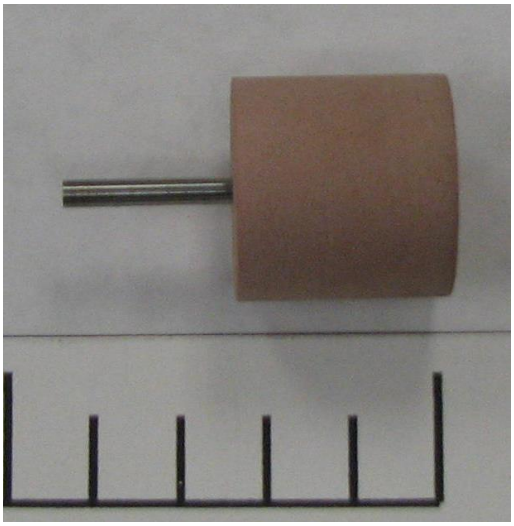

**Fig. 9 Rod projectile**

## 3. Results and Discussion

Prior to examining the ballistic behavior of the alumina materials, the density, hardness, quasi-static flexural strength, and microstructure were determined. Rod-shaped specimens, nominally 3 mm in diameter and 50 mm long, were obtained for

each alumina. The density was determined using the Archimedes method, the flexure strength was determined following the guidelines in ASTM C1684,[7] and the Knoop Hardness at 2,000 g according to ASTM C1326.[8] Table 1 summarizes these data and Fig. 10 shows the microstructure of each alumina. These alumina materials appear similar based on this information. The pore density appears higher in the CoorsTek alumina, and the maximum pore size is larger in the HEW, with some cracks connecting neighboring pores. The HEW alumina is only 0.03 ± 0.08 g/cm$^3$ less dense than the CoorsTek.

**Table 1 Property summary**

| Material | Density (g/cm$^3$) | Flexure strength (MPa) | Knoop hardness - $HK_2$ (GPa) |
|---|---|---|---|
| CoorsTek AD-995 | 3.92 ± 0.00 | 162 ± 54 | 13.2 ± 1.3 |
| HEW | 3.89 ± 0.08 | 130 ± 38 | 14.7 ± 1.0 |

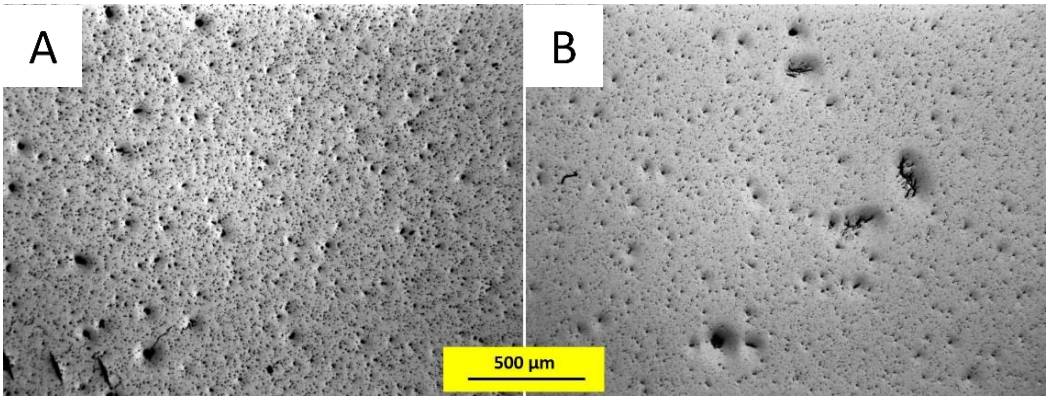


**Fig. 10 Representative microstructure of A) AD-995 and B) HEW alumina**

A few shots were fired into monolithic AA6061 plates over the velocity range from 824 to 872 m/s (2,704 to 2,861 ft/s) to quantify the DOP without the ceramic, as shown in Fig. 11.[9] The primary penetrator defeat mechanism of AA6061 over the velocity regime was deceleration. Residual penetration values were then measured and plotted as a function of striking velocity to produce a baseline curve (Fig. 12). A linear regression of the reference data yielded the following equation:

$$DOP = 0.1959 \times V_{x\text{-}ray} - 84.406. \quad (1)$$

The square of the correlation coefficient, $R^2$, is 0.946, indicating that this curve is a reasonable approximation. For example, an experimental impact velocity of 848 m/s would be expected to result in a DOP of 81.73 mm. For these experiments, this is the DOP baseline for AA6061.

| $V_{x\text{-}ray}$ (m/s) | Plate 1 (front plate) | Plate 2 |
|---|---|---|
| 848 |  |  |
| 824 |  | 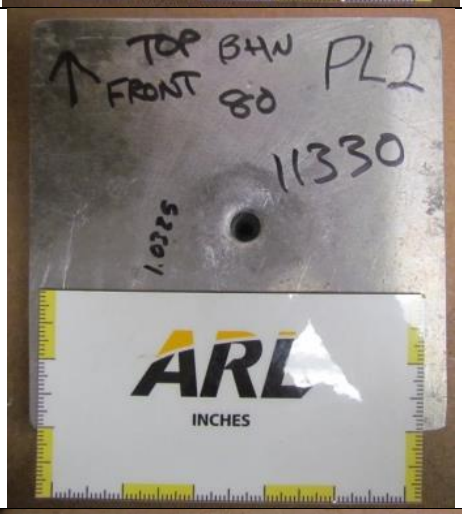 |
| 872 |  |  |

**Fig. 11 Ballistic penetration into AA6061**

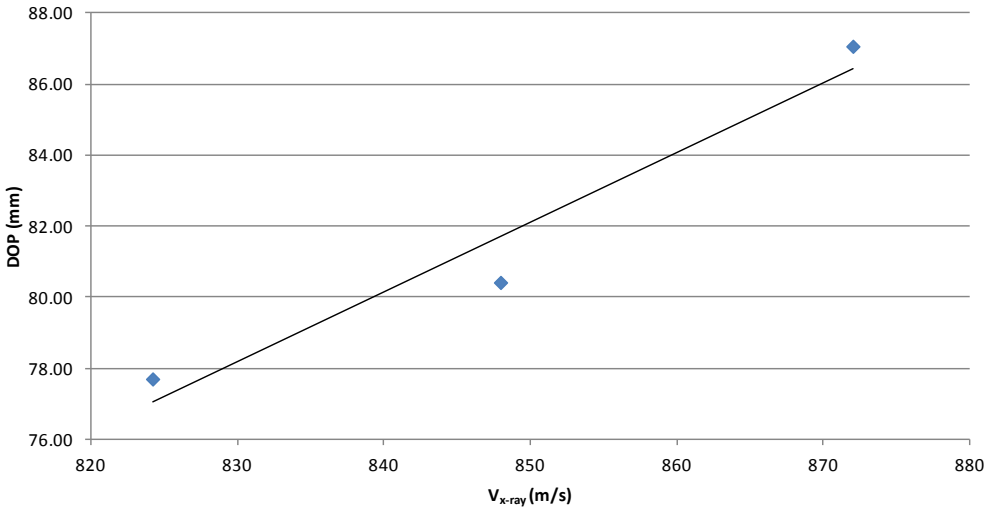


**Fig. 12 Penetration of 12.7-mm APM2 into AA6061**

Ceramic target assemblies, as previously described in Section 2, were fabricated for all materials. In general, 3 tiles of equal thickness (or areal density) were evaluated for each material. To adjust for variations in the actual strike velocity, all residual penetration values were normalized to a striking velocity of 848 m/s based on the empirical fit shown in Eq. 1. The correction was made as follows:

$$\text{Corrected DOP} = \text{Measured DOP} + [0.1959 \times (848 - V_{x\text{-ray}})] \; . \qquad (2)$$

This technique has been found to be valid provided that a significant amount of the penetrator reaches the backup plate, the correction is relatively small, and that the penetrator defeat mechanism has not significantly changed with velocity.[9] In support of this assumption, observations of the size and shape of the impact showed no significant differences in penetrator cavity for the impact velocity variations. The data were obtained for the alumina tiles at a nominal thickness of 8 mm. The ballistic impact measurements are listed in Table 2. The average DOP with the correction for the AD-995 was 14.43 mm with a standard deviation of 3.01 mm. The average DOP with the correction of the HEW alumina was 24.01 mm with a standard deviation of 2.06 mm. The difference between the HEW and CoorsTek was 9.58 mm, which is equivalent to about three-quarters of the diameter of the projectile, or one-sixth of the length of the projectile.

**Table 2 Ballistic impact measurements for alumina tiles**

| Shot no. | Ceramic alumina type | Striking velocity (m/s) | Pitch (°) | Yaw (°) | Total yaw (°) | DOP (mm) | $DOP_{corr}$ (mm) |
|---|---|---|---|---|---|---|---|
| 13157 | AD-995 | 840 | 0.47 | –0.62 | 0.78 | 16.00 | 17.56 |
| 13158 | AD-995 | 843 | 0.61 | –0.39 | 0.72 | 13.21 | 14.18 |
| 13159 | AD-995 | 846 | 0.26 | –0.48 | 0.54 | 11.18 | 11.56 |
| 13160 | HEW | 860 | 0.51 | –0.50 | 0.72 | 28.70 | 26.34 |
| 13161 | HEW | 850 | 0.31 | –0.58 | 0.65 | 23.62 | 23.22 |
| 13162 | HEW | 850 | 0.32 | –0.46 | 0.56 | 22.86 | 22.46 |

In these limited experiments, the AD-995 tiles caused more damage to the penetrator than the HEW alumina tiles. It was interesting to observe for each ceramic composite that the DOP increased as yaw increased. More experiments would need to be conducted to determine if this response was a coincidence or a phenomena. The penetrator underwent 2 failure mechanisms, fragmentation and erosion, when it impacted the AD-995 tiles, as shown in Fig. 13. The penetrator underwent one failure mechanism, erosion, when it impacted the HEW alumina tiles, as shown in Fig. 14. The residual projectile cores (when recovered) were measured and a curve fit was calculated (Figs. 15 and 16). It was likely that not all of the debris was recovered upon the projectile shattering and/or eroding on impact. The length of the largest piece was measured as the residual penetrator length. The length for shot no. 13159 was not captured because only small fragments of the projectile were recovered. The mass of the recovered core fragments were measured. The unaltered core was added to the figure as a point of reference at the striking velocity of 825 m/s.


**Fig. 13 Residual penetrator from impact versus CoorsTek alumina AD-995**


**Fig. 14 Residual penetrator from impact versus HEW alumina**

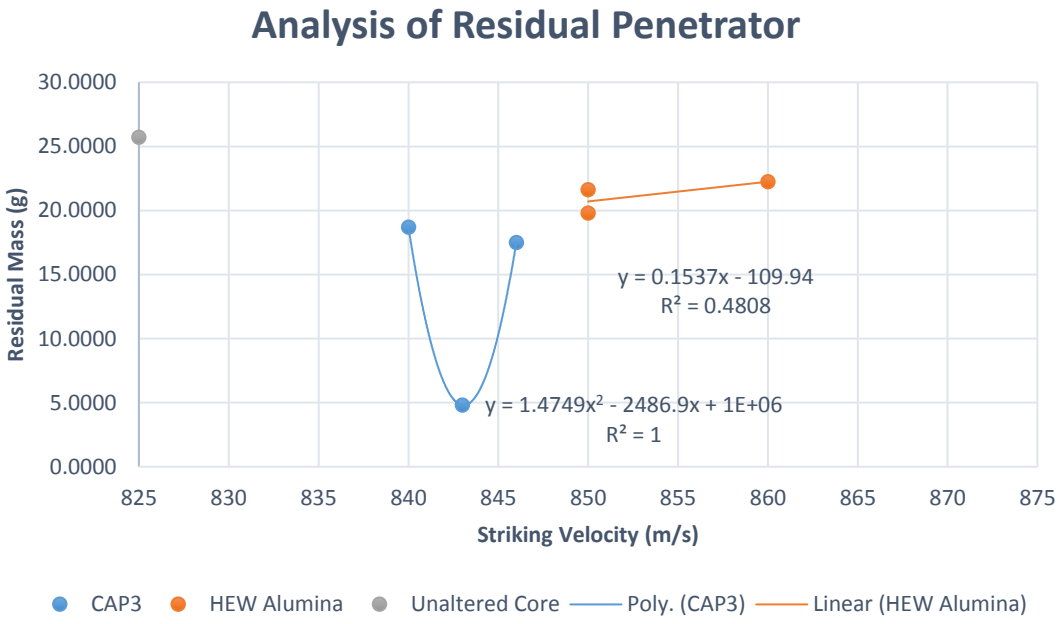


**Fig. 15 Residual mass of 12.7-mm APM2 into AA6061**

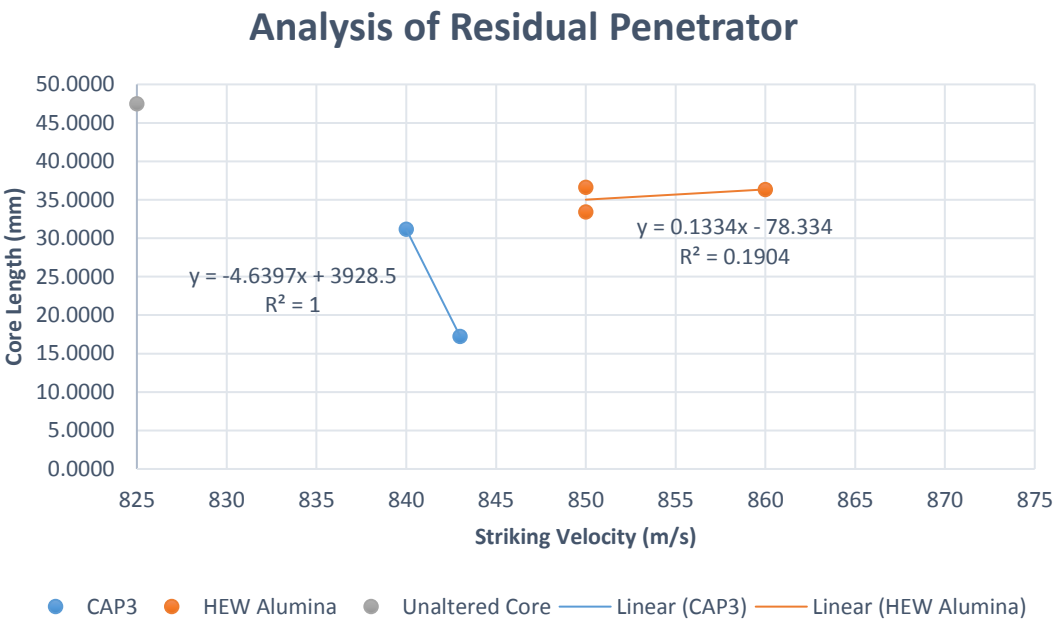


**Fig. 16 Residual length of 12.7-mm APM2 into AA6061**

The postexperimental targets were optically examined for ceramic failure analysis; typical ceramic failures are shown in Figs. 17 and 18. The CoorsTek and HEW alumina both started failing with tensile fracture, then continued into comminution to dissipate the energy of the penetrator. The extent of the ceramic damage was very similar for both types of alumina. However, the DOP cavity profile into the AA6061 plates were distinctly different.


**Fig. 17 CoorsTek alumina AD-995 after impact**

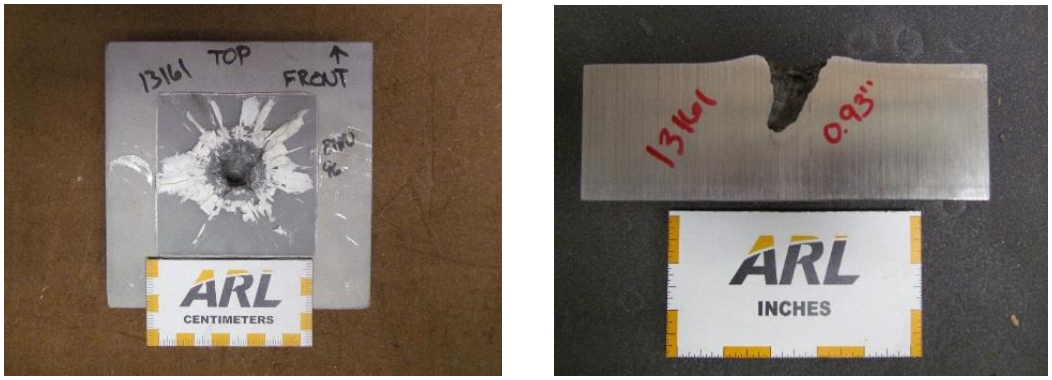


**Fig. 18 HEW alumina after impact**

During the ballistic impact, the CoorsTek alumina typically fractured the penetrator into 2 large pieces and some small chips before starting the erosion process. As a result there were 2 projectile canals into the AA6061 plate. The HEW alumina did not fracture the penetrator and only eroded the penetrator. As a result there was one residual penetrator canal into the AA6061 plate.

Since AA6061 was the reference material used in this study, Eq. 3 was used to provide a coefficient of performance ($C_p$) of the ceramics compared to the reference material:

$$C_p = \left(\rho_{AA6061}\right)\frac{DOP_{Base\_AA6061} - DOP_{Corr\_AA6061}}{AD_{Ceramic}}, \tag{3}$$

where $DOP_{Base\_AA6061}$ is the average expected residual depth of penetration into bare aluminum at 848 m/s; $DOP_{Corr\_AA6061}$ is the residual DOP into AA6061 after perforating the ceramic tile, corrected for the variations in striking velocity; and $AD_{ceramic}$ is the areal density of the ceramic. The $DOP_{Base\_AA6061}$ = 81.73 mm. The $AD_{AD\text{-}995}$ = 31.36 kg/m$^2$ and the $AD_{HEW\_Alumina}$ = 31.12 kg/m$^2$. The $\rho_{AA6061}$ = 2.70 g/cm$^3$. The calculated $C_p$ value provides a relative comparison of the ceramic with AA6061 (i.e., a $C_p$ of 5 means the ceramic is 5 times more weight effective than AA6061). The $C_p$ of each alumina ceramic was calculated as shown in Table 3. A ceramic performance map is illustrated in Fig. 19. Clearly, the CoorsTek alumina has superior performance versus the HEW.

**Table 3 Comparative performance of ceramics**

| Experiment no. | Coefficient of performance ($C_p$) | |
|---|---|---|
| | CoorsTek AD-995 | HEW alumina |
| 1 | 5.52 | 4.81 |
| 2 | 5.82 | 5.08 |
| 3 | 6.04 | 5.14 |

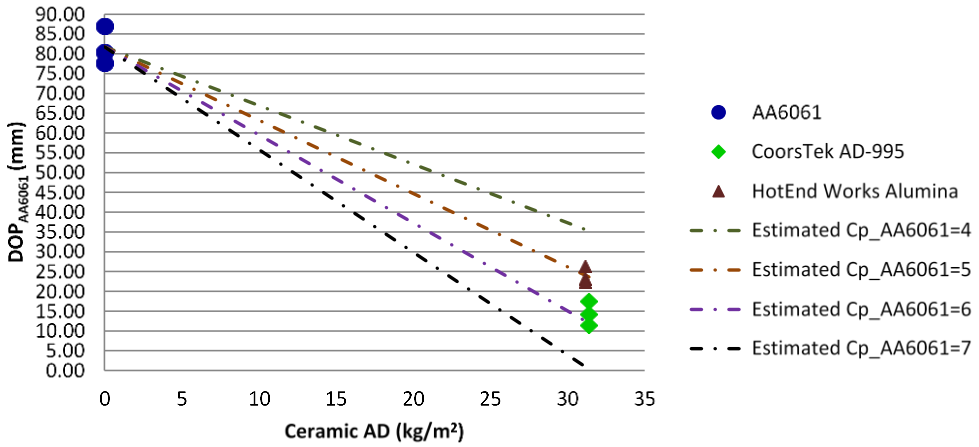


**Fig. 19 Ceramic performance map**

The progressive failure through brittle fracture of the 6-mm-thick ceramic samples with no backing plate are shown in Fig. 20. The projectile velocities were 206 and 214 m/s for the CoorsTek and HEW alumina samples, respectively. The series of images are right before impact and 10, 40, 90 and 200 μs after impact. They show similar overall features. Concentric cracks appear first, several microseconds after impact, then radial cracks appear. The concentric cracks at the back-face probably form a cone crack through the thickness of the sample, but it cannot be seen because the alumina is opaque. After 90 μs the concentric cracks have clearly coalesced because the inner material has been pushed out by the rod to a greater extent than the material near the outer edge. At 200 μs both samples look similar but the HEW alumina appears to have fragmented slightly more. The biggest difference between the 2 materials is that the CoorsTek has less radial cracks than the 3-D printed material. Additionally, after 90 μs the area within the concentric cracks of the HEW alumina has further cracked and started to break up, while the same region of the CoorsTek has not cracked any further. A summary of the dynamic failure modes is shown in Table 4.

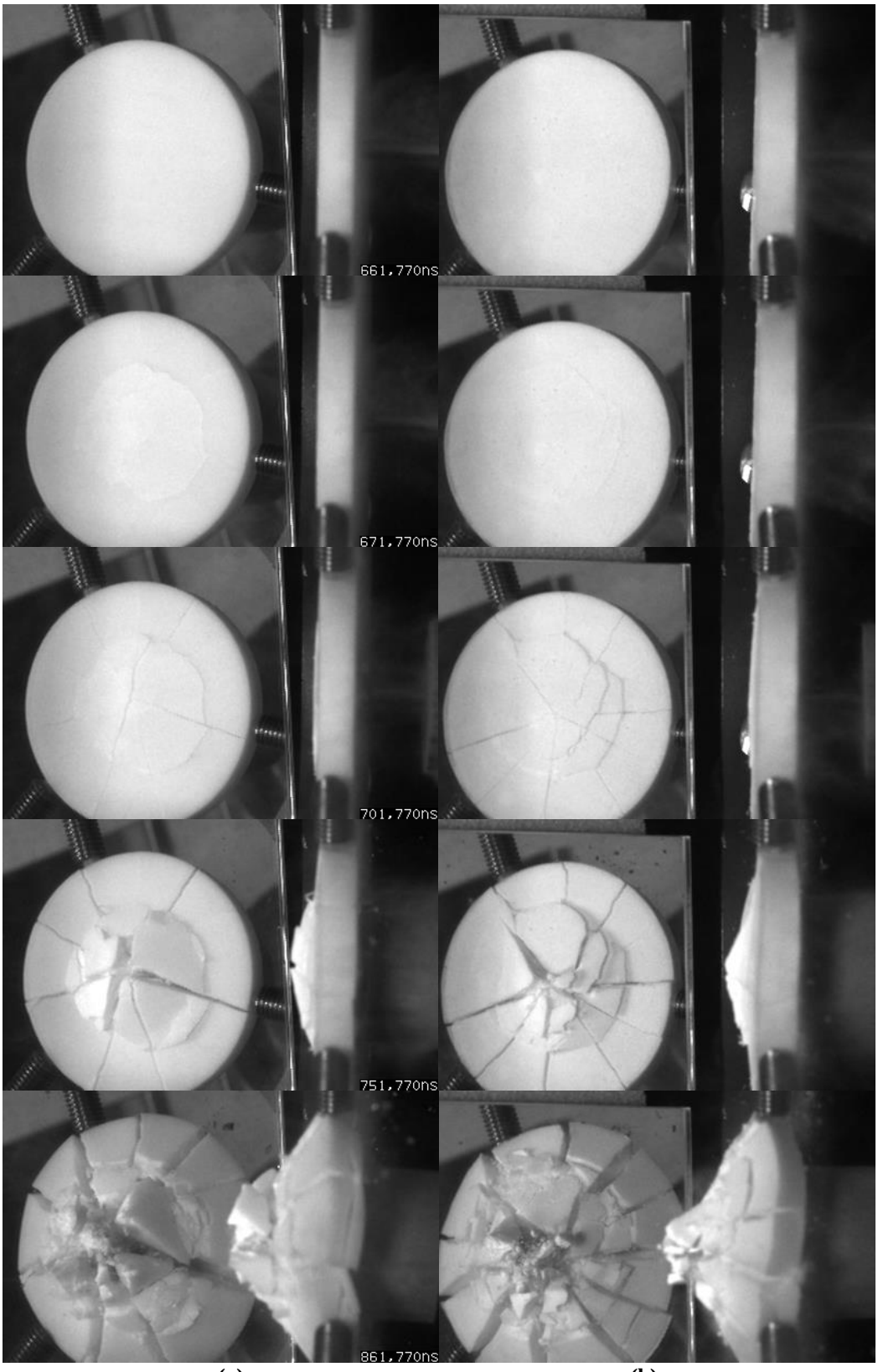


**(a)** **(b)**

**Fig. 20 Progressive fracture of the 6-mm ceramic: a) CoorsTek and b) HEW**

**Table 4 Comparison of the dynamic failure modes of 6-mm-thick alumina discs**

| Time interval (μs) | CoorsTek AD-995 | HEW 3-D printed alumina |
|---|---|---|
| Preimpact, 0 | Disc intact | Disc intact |
| Postimpact, 10 | Radial-forming cracks | Radial-forming cracks |
| Postimpact, 40 | Longitudinal cracks forming | Longitudinal cracks forming |
| Postimpact, 90 | 7 longitudinal cracks that run from center to edge of disc; plugging with discrete fragments forming | 9 longitudinal cracks that run from center to edge of disc; plugging with comminution process beginning |
| Pos-impact, 200 | Fragmentation process is converting into the comminution process | Comminution process is occurring |

Figure 21 shows the progression of failure of the 8-mm-thick samples with projectile velocities of 216 and 224 m/s. The time is right before impact and after 10, 40, 90 and 200 μs, respectively, in the series of images, which is the same as in Fig. 20. As before, the overall features between the 2 are similar. The 8-mm-thick samples show very few concentric cracks at any time following impact. Radial cracks are the first damages to appear. As expected, it takes longer for cracks to emerge on the backside of the samples, and the damage at the same time after impact is less with the thicker samples. Also, there are fewer radial cracks with the CoorsTek versus the HEW alumina. At a couple hundred microseconds after impact, the HEW alumina has fragmented to a greater extent. A summary of the dynamic failure modes is shown in Table 5. Videos that detail the dynamic failure modes during each of these rod impact tests, Tests 1 and 6 for the performance of the 6-mm-thick tiles and Tests 3 and 4 for the performance of the 8-mm-thick tiles, are included in the Appendix of this report.

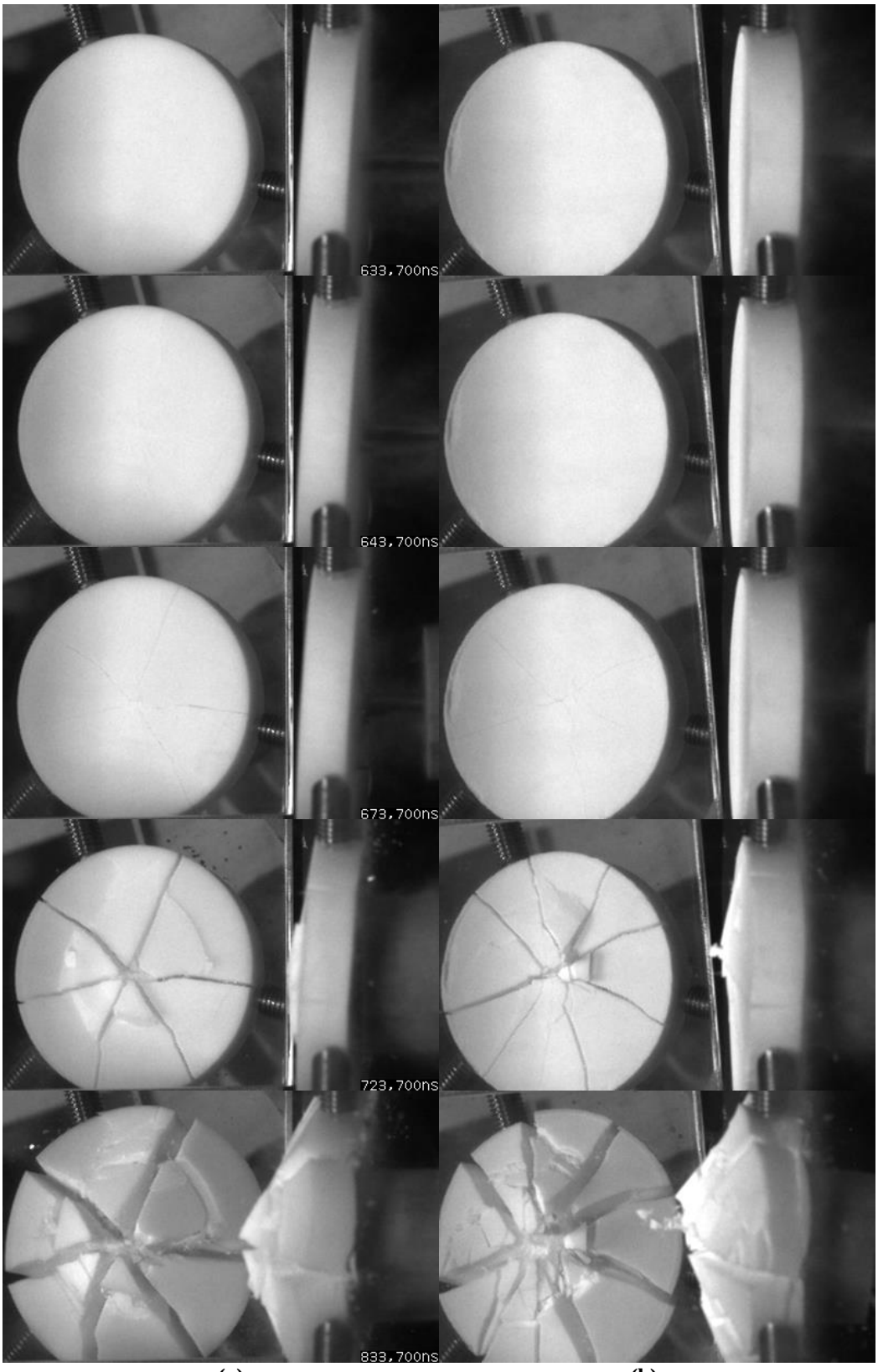


**Fig. 21 Progressive fracture of the 8-mm ceramic: a) CoorsTek and b) HEW**

**Table 5 Comparison of the dynamic failure modes of 8-mm-thick alumina discs**

| Time interval (μs) | CoorsTek AD-995 | HEW 3-D printed alumina |
|---|---|---|
| Preimpact, 0 | Disc intact | Disc intact |
| Postimpact, 10 | Disc intact | Disc intact |
| Postimpact, 40 | Longitudinal cracks forming | Longitudinal cracks forming |
| Postimpact, 90 | 6 longitudinal cracks that run from center to edge of disc; plugging mode beginning; discrete fragments forming | 8 longitudinal cracks that run from center to edge of disc; no plugging mode; comminution process is beginning |
| Postimpact, 200 | Fragmentation process is transforming into the comminution process | Comminution process is occurring |

## 4. Conclusions

This program was a preliminary investigation into the viability of using a 3-D printed alumina ceramic for body armor applications. The coefficient of performance showed that CoorsTek alumina AD-995 was 13% more efficient against ballistic penetration than the HEW alumina tiles. Initial clues as to why were provided by the low-velocity, rod impact experiments into unbacked ceramic discs. These exploratory experiments showed there is a critical thickness limit at a given velocity that is needed to simulate the realistic failure modes of the alumina ceramic under ballistic impact. In the 6-mm-thick ceramic tile experiments, the rod impact exhibited more plugging mode failure, which is not desirable in conventional armor strategy. In the 8-mm-thick ceramic tile experiments, the HEW alumina had a greater number of radial cracks and fragmented to a greater extent than the CoorsTek alumina. The disc diameters were adequate for the low-velocity rod impact. The 3-D deposition process will need to be improved to reduce the pore size and increase the flexural strength of the 3-D printed ceramic material. Improvements to the sintering method will be the critical correlation to the improvements in the ceramic failure mechanisms and the penetrator failure mechanisms during low-velocity rod impacts and the ballistic penetrator impacts. It is imperative that Hugoniot shock pressure limit experiments be conducted. At pressures just above the elastic limit on the Hugoniot, called the Hugoniot elastic limit (HEL), a shock wave is split into a 2-wave structure by the HEL, which is determined by strength.[10] Up to the HEL, a single, elastic, supersonic shock wave propagates. At higher pressures, shock compression causes plastic deformation as well. A solid just above its HEL is softer (more compressible) than it is below its HEL. By measuring time-resolved shock wave profiles, HELs, mechanical

constitutive properties, and equations of state are derived.[10] Then quantifying the fracture behavior between these ceramics manufactured by different methods can be analytically predicted. The successful implementation of these steps, including the initial correlation between these dynamic variables and the manufacturing process variables, are expected to elevate the 3-D printed ceramic static, quasi-static, and dynamic properties to match, or exceed, those of conventionally sintered alumina.

## 5. References


1. King A. Ceramic technology and processing. 1st ed. Norwich (NY): William Andrew Publishing; 2002.

2. Becker B. Additive changes to advanced ceramics. Ceramic Industry; 2014 Apr 10. [accessed 2016 May 10]. http://www.ceramicindustry.com/articles /93848-additive-changes-to-advanced-ceramics.

3. Woolsey P, Kokidko D, Mariano S. Alternative test methodology for ballistic performance ranking of armor ceramics. Watertown (MA): Army Materials Technology Laboratory (US); 1989. Report No.: MTL-TR 89-43.

4. MIL-STD-662F. V50 ballistic test for armor. Aberdeen Proving Ground (MD): Army Research Laboratory (US); 1997 Dec 18.

5. MIL-DTL-32262. Armor plate, aluminum alloy, unweldable applique 6061. Aberdeen Proving Ground (MD): Army Research Laboratory (US); 2007 July.

6. Jones, T. Investigation of the kinetic energy characterization of advanced ceramics. Aberdeen Proving Ground (MD): Army Research Laboratory (US); 2015 Apr. Report No.: ARL-TR-7263.

7. ASTM C1684. Standard test method for flexural strength of advanced ceramics at ambient temperature-cylindrical rod strength. West Conshohocken (PA): ASTM International; 2008.

8. ASTM C1326. Standard test method for Knoop indentation hardness of advanced ceramics. West Conshohocken (PA): ASTM International; 2013.

9. Jones T. Investigation of the kinetic energy characterization of advanced ceramics. Aberdeen Proving Ground (MD): Army Research Laboratory (US); 2015 Apr. Report No.: ARL-TR-7263.

10. Nellis, WJ. Dynamic compression of materials: Metallization of fluid hydrogen at high pressures. Reports on Progress in Physics. 2006;69(5):1479.

INTENTIONALLY LEFT BLANK.

# Appendix. Videos

Rod Impact Test Description

- Test 1: 6-mm-thick CoorsTek AD-995 alumina disc at 205.6 m/s
- Test 2: 6-mm-thick HEW 3-D printed alumina disc at 227.9 m/s (the triggering was off so the first image is after impact occurred)
- Test 3: 8-mm-thick CoorsTek AD-995 alumina at 215.9 m/s
- Test 4: 8-mm-thick HEW 3-D printed alumina at 233.6 m/s (the triggering was off so the first image is after impact occurred)
- Test 5: 8-mm-thick HEW 3-D printed alumina at 224.3 m/s (this essentially replaces Test 4)
- Test 6: 6-mm-thick HEW 3-D printed alumina at 213.9 m/s (this essentially replaces Test 2)

Click on the icon arrow to view the video for each test.


TEST1~1.MP4


TEST2~1.MP4


TEST3~1.MP4


TEST4~1.MP4


TEST5~1.MP4


TEST6~1.MP4

## List of Symbols, Abbreviations, and Acronyms

3-D 3-dimensional

DOP depth of penetration

EDM electrical discharge machining

HEL Hugoniot elastic limit

HEW HotEnd Works, LLC

PSD pressurized spray deposition

1 (PDF) DEFENSE TECHNICAL INFORMATION CTR DTIC OCA

2 (PDF) DIRECTOR US ARMY RESEARCH LAB RDRL CIO L IMAL HRA MAIL & RECORDS MGMT

1 (PDF) GOVT PRINTG OFC A MALHOTRA

3 (PDF) ALCOA R KANE D MOOY J CARATELLI

1 (PDF) ALERIS L KRAMER

1 (PDF) AMERICA MAKES, NAT ADD MFG INNOV INST M RICHMOND

3 (PDF) CONSTELLIUM P KOBE M NIEDZINSKI M PHILBROOK

1 (PDF) KAISER J SCHEURING

1 (PDF) NSWC R PETERSON

4 (PDF) BAE SYSTEMS J DORSCH B KARIYA D SCHADE M MIDDIONE

1 (PDF) GDLS W HERMAN

1 (PDF) HOTEND WORKS B BECKER

1 (PDF) WA GOOCH CONSULT INC W GOOCH

1 ((PDF) PENN STATE UNIV D SWANSON

1 (PDF) CELLULAR MTRLS INTRNTL INC Y MURTY

1 (PDF) R3 TECHNOLOGY INC J RIEGEL

1 (PDF) UNIV OF VIRGINIA H WADLEY

1 (PDF) RJ TECHNOLOGIES R JONES

2 (PDF) ATEC K BEAVERS J WHITE

8 (PDF) TARDEC A SOCKS J PEREZ F RICKERT C FILAR R TRANCYGIER M MCDONNEL M ROGERS D TZELEPIS

2 (PDF) PEO GCS T DEAN D SPENSER

1 (PDF) OSHKOSH DEFENSE M RICHMOND

2 (PDF) SOC OF MFG ENGINEERS C MITROFF A KALERGIS

5 (PDF) RDECOM W EVERETT R IMPERIALE S CLARK A DAVIS D SKELTON

2 (PDF) OFC OF THE DPTY ASSIST SECY OF DEFNS FOR EMERGING CAPIBILITY & PROTOTYPING E WYATT R THOMPSON

1 (PDF) US NAVY RSRCH LAB J MORAN

1 (PDF) NSWC CARDEROCK DIV
E TRUEMAN

2 (PDF) DOD CORROSION POLICY AND OVERSIGHT OFC
R HAYS
D DUNMIRE

1 (PDF) OFC OF THE DIR DEFNS RSRCH AND ENGRG
L SLOTER

1 (PDF) USMC CORROSION PREVENTION AND CNTRL
A SHEETZ

2 (PDF) PEO SOLDIER
J ZHENG
V HALLS

1 (PDF) USSOCOM
C LOVELL

3 (PDF) NSRDEC
J KIREJCZYK
D COLANTO
J WARD

7 (PDF) US ARMY ARDEC
J KRAFT
D CLARK
J ZUNINO
J SCHUTZ
J WARD
D COLANTO
J KIREJCZYK

1 (PDF) PEO CS CSS
S LEFEBVRE

4 (PDF) AMRDEC
V LEFEVRE
J WHITE
K OLSON
E MARTIN

1 (PDF) SMI
T MCGREGOR

3 (PDF) CASCOM
J PINSON
R LAIR
L SHEPPARD

1 (PDF) PEO AVN
J METZGER

1 (PDF) PEO AMMO
V MATRISCIANO

2 (PDF) AMC
R FOLEY
Y CHEN

1 (PDF) HQDA DCA DCS
S SEITZ

1 (PDF) HQDA ASA ALT
N FORTIER

1 (PDF) TACOM
T POLLARD

1 (PDF) US ARMY REF
S DELGADO

1 (PDF) MANTECH
S LUCKOWSKI

1 (PDF) US ARMY AC
C LIM

1 (PDF) UNIV SLTNS INTRNTL INC
D SZCZUR

1 (PDF) USAF
A SCHRAND

2 (PDF) US ARMY ECBC
R MOORE
K WALLACE

1 (PDF) NAVSCOLEOD
T SEAMAN

2 (PDF) NASA
J GARDNER
E SIOCHI

1 (PDF) USN NAVAIR WAREFARE CTR AC
E MCMICHAEL

2 (PDF) USAF AFRL MTRLS
J MILLER
M KINSELLA

1 (PDF) US ARMY ORDNANCE SCHL
B SUMMERFIELD

1 (PDF) USN
J WOLK

1 (PDF) SOUTHWEST RSRCH INST
K DANNEMANN

1 (PDF) GS TECHLGYS
G SILSBY

1 (PDF) RENSSELAER POLY INST
S A JACKSON

46 (PDF) DIR USARL
RDRL D
J MAIT
T RUSSELL
P PERCONTI
RDRL RO
S LEE
RDRL SL
P BAKER
RDRL WM
J MCCAULEY
J ZABINSKY
B FORCH
S KARNA
J LASCALA
RDRL WML
M ZOLTOSKI
P PEREGINO
RDRL WML B
R PESCE-RODRIGUEZ
RDRL WML H
L MAGNESS
T EHLERS
J NEWILL
RDRL WMM
M VANLANDINGHAM
R DOWDING
RDRL WMM C
B PLACZANKIS
RDRL WMM D
B CHEESEMAN
R SQUILLACIOTI
R CARTER
M KORNECKI
RDRL WMM E
M BRATCHER
J SINGH
J LASALVIA
J SWAB
RDRL WMM F
K DOHERTY
J CHINELLA
S GRENDAHL
RDRL WMP
D LYON
RDRL WMP B
C HOPPEL
RDRL WMP C
T BJERKE
J CLAYTON
C MEREDITH
D CASEM
R WORTHINGSTON
RDRL WMP D
J RUNYEON
D PETTY
RDRL WMP E
M BURKINS
E HORWATH
T JONES
P SWOBODA
E KLIER
RDRL WMP F
N GNIAZDOWSKI
RDRL WMS
H MAUPIN